LAWRENCE
LIVERMORE
NATIONAL
LABORATORY

LLNL-PROC-560180

Humidity Tolerance of Electrochemical Hydrogen Safety Sensors Based on Yttria-Stabilized Zirconia (YSZ) and Tin-doped Indium Oxide (ITO)

L. Y. Woo, R. S. Glass, E. L. Brosha, R. Mukundan, F. H. Garzon, W. J. Buttner, M. B. Post, C. Rivkin, R. Burgess

June 7, 2012

Electrochemical Society Meeting
Seattle, WA, United States
May 7, 2012 through May 11, 2012

Disclaimer

LLNL-PROC-560180

Humidity Tolerance of Electrochemical Hydrogen Safety Sensors Based on Yttria-Stabilized Zirconia (YSZ) and Tin-doped Indium Oxide (ITO)

L.Y. Woo[a], R.S. Glass[a], E.L. Brosha[b], R. Mukundan[b], F.H. Garzon[b], W.J. Buttner[c], M.B. Post[c], C. Rivkin[c], and R. Burgess[c]

[a] Lawrence Livermore National Laboratory, Livermore, California 94551, USA
[b] Los Alamos National Laboratory, Sensors and Electrochemical Devices Group, Los Alamos, New Mexico, USA
[c] National Renewable Energy Laboratory, Hydrogen Technologies and Systems Center, Golden, CO 80401, USA

Commercial hydrogen sensors are available, but performance and cost targets remain unmet for many hydrogen economy applications. For example, traditional thermal conductivity detectors (TCDs) can be responsive to combustible gases in general, show humidity effects, and are relatively costly. New options under development include solid-state electrochemical sensors, which are low cost, can be operated over various temperature and humidity ranges, have fast response times, and can show low cross-sensitivity to hydrocarbons. Previous work demonstrated potentiometric sensors based on yttria-stabilized zirconia (YSZ) and tin-doped indium oxide (ITO). In this study, prototypes were investigated for humidity tolerance. Electrochemical characterization indicated similar reaction rates for negative and positive potentials could be important for humidity tolerance. More advanced prototypes were developed to demonstrate miniaturization and robust packaging for cross-validation testing. Additional electronics were developed for compatibility with data acquisition systems, and results validated humidity tolerance for H_2 sensors up to 10% water in air.

Introduction

Hydrogen sensors are increasingly important for existing as well as emerging energy applications where hydrogen acts as a versatile energy carrier. For human safety and to ensure infrastructure reliability, sensors are needed to monitor hydrogen gas, which, when mixed with air, is flammable in the range of 4-75 vol%. In safety applications, sensors are required for detecting unintentional release or leaks. The availability of low-cost reliable hydrogen safety sensors will encourage wider acceptance of hydrogen as a clean and sustainable energy carrier.

A number of commercial hydrogen safety sensors are currently available on the market; however, performance gaps still exist and improvements are necessary to meet all the desired technical requirements (1-2). Desired technical performance requirements vary depending on the application, but in general include:

- sensitivity to H_2 at least in the 1-4 vol% range in air
- lifetime up five years with no, or minimal calibration
- desired accuracy of ±1% full scale in the range of 0.04-4 vol%
- capable of operating in ambient conditions from of -40 °C to 60 °C
- response time of < 1 min at 1 vol% and < 1 sec at 4 vol% with a recovery time of < 1 min
- low cross-sensitivity to humidity, H_2S, CH_4, CO, and VOCs

Also, cost targets need to be met in order to enable wider adoption. Electrochemical solid-state sensors have the ability to be produced at low cost, as evidenced by the widely used oxygen exhaust gas sensor. Also, solid-state electrochemical technology is well suited for meeting more stringent requirements including operation over a wide temperature range for different hydrogen applications, fast response times, low cross-sensitivity to hydrocarbons, and reliability under variations in humidity. Previous work has demonstrated the potential for potentiometric electrochemical solid-state safety sensors based on a yttria-stabilized zirconia (YSZ) electrolyte, tin-doped indium oxide (ITO) sensing electrode, and Pt counter electrode (ITO/YSZ/Pt) (3-6).

Two distinct operational modes for electrochemical sensors are amperometric and potentiometric, where the sensing signal is then either the current or voltage respectively. Our work has focused on potentiometric operation. In this approach, the two electrodes are both in contact with the YSZ, an oxygen-ion conducting electrolyte, and both electrodes are exposed to the test gas, which consists of various concentrations of hydrogen in air. Reactions for different species, including the oxygen and hydrogen/water oxidation/reduction reactions (shown in Eqs. 1 and 2, respectively), occur at both electrodes and can result in a cell potential as measured by the open circuit voltage (see Fig. 1). The largest magnitude sensor response would be expected when one electrode responds preferentially to changes in hydrogen concentration relative to the opposing electrode, an effect that is influenced by material composition, microstructure, and sensor geometry. This results in what is referred to as a mixed potential sensor (7).

$$\tfrac{1}{2}\, O_2 + 2e^- \leftrightarrow O^{2-} \qquad [1]$$

$$H_2 + O^{2-} \leftrightarrow H_2O + 2e^- \qquad [2]$$

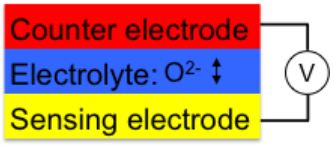

Figure 1. Configuration for electrochemical cell in potentiometric operation with two electrodes, both in contact with the oxygen-ion conducting electrolyte and the sampled gas.

In this study, humidity tolerance was investigated for an electrochemical cell that consisted of only oxide materials, including a YSZ-ITO composite sensing electrode, a YSZ electrolyte, and a strontium-doped lanthanum manganite (LSM) counter electrode. For cells that only consist of oxide materials, co-sintering manufacturing processes could

be used to reduce costs, with additional cost reduction advantages from eliminating precious metals. In parallel efforts, an advanced prototype was developed to demonstrate miniaturization and for cross-verification testing on the specialized humidity test stand developed by the National Renewable Energy Laboratory (NREL) for evaluating commercial and pre-commercial hydrogen safety sensors.

Experimental

The structure of the YSZ-ITO/YSZ/LSM and Au/YSZ/Pt cells used in this investigation are shown in Fig. 2. These sensors were fabricated using bulk processing techniques including spin coating of a YSZ slurry that consisted of YSZ powder (Tosoh Corp., 8 mol% Y_2O_3-doped ZrO_2) mixed with ethanol, binder (polyvinyl butyral, Butvar), dispersant (phosphate ester), and plasticizer (dipropylene glycol dibenzoate). The cells were supported on alumina substrates (10 mm × 10 mm × 0.5 mm, Valley Design Corp.) that were suitable for controlled temperature furnace testing. While not used in this work, more advanced sensors will feature alumina substrates with embedded heating elements.

Figure 2. Schematic of electrochemical cells for laboratory evaluation including (a) a cell with only oxide materials, YSZ-ITO/YSZ/LSM, and (b) a cell with metal electrodes, Au/YSZ/Pt.

For the cell with only oxide materials (ITO-YSZ/YSZ/LSM), the composite ITO-YSZ sensing electrode was fabricated using an impregnation technique. ITO was added, using a low-temperature solution procedure, to a porous YSZ structure made by spin coating YSZ slurry and firing to 900 °C. The impregnation solution consisted of 5 wt% ITO nanocrystalline powder (average particle size ~20 nm) in a colloidal suspension of 50 wt% ethanol in water. YSZ slurry was then spin coat on top of the composite ITO-YSZ sensing electrode. The top LSM counter electrode was fabricated using a dense pellet prepared with commercial $(La_{0.85}Sr_{0.15})_{0.98}Mn$ oxide powder (Praxair) by pressing powder in a uniaxial die and sintering at 1250 °C. The LSM pellet was then machined to 6 mm × 2 mm × 1 mm and attached to the top of the YSZ slurry with conductive paste, and the cell was fired for two hours at 900 °C. Electrical contact to the electrodes was made using platinum ink (Engelhard 6082).

For the Au/YSZ/Pt prototype, the counter electrode was formed using platinum ink that was applied to the substrate and fired for two hours at 1200 °C. YSZ slurry was then spin coated on top of the platinum counter electrode. A Au wire electrode (0.25 mm diameter) was attached to the top of the YSZ slurry and additional slurry applied on top of the wires. The assembled prototype was fired for two hours at 1000 °C.

Laboratory gas sensing experiments were performed in a quartz tube placed inside a tube furnace with both electrodes exposed to the same environment. Gas composition was controlled by mixing air and hydrogen feed using a gas handling system equipped with thermal mass flow controllers. The total gas flow rate was fixed at 200 mL/min. Water concentration was controlled using a heated water injection system with a liquid flow controller to achieve water concentrations of up to 10%. Measurements in the furnace were performed at 600 °C. The experimental protocol for evaluating sensor performance included dynamic 2.5 min steps of increasing and then decreasing hydrogen concentrations from 0, to 0.25, 0.5, 1, 2% in both dry and humid air with 10% water. Laboratory electrochemical measurements were performed using either a Modulab Electrochemical Test System (Solartron Analytical) or a VoltaLab 40 Dynamic Electrochemical Laboratory Instrument (Radiometer Analytical). Both impedance spectroscopy and cyclic voltammetry were used to characterize the steady-state behavior with and without hydrogen, under dry and humid conditions. Impedance spectra were obtained using an excitation voltage of 100 mV over the frequency range of either 1 MHz or 100 kHz to 1 Hz at 10 steps per frequency decade. Cyclic voltammetry was performed using applied potentials from 250 to -250 mV with scan rates of 10, 50, and 100 mV/sec.

In parallel work, an advanced prototype was also developed to demonstrate miniaturization, to incorporate an on-chip embedded resistive heater, and to interface to a custom built high input impedance buffer board for signal collection. The experiments for this sensor package were conducted using the specialized humidity test stand at the National Renewable Energy Laboratory (NREL). This facility is used for evaluating commercial and pre-commercial hydrogen safety sensors. The more advanced prototypes used an alumina substrate (4 mm × 4 mm × 1 mm) with an embedded Pt resistive heating element, and a Pt counter electrode and contact pads, which were fabricated by ESL ElectroScience (King of Prussia, PA). RF magnetron sputter deposition was then used to deposit the thin film ITO electrode, and electron beam evaporation was used to deposit the thin film YSZ electrolyte (see Fig. 3a). The sensor was placed within a MACOR housing with leads attached to the sensors and heater (see Fig. 3b).

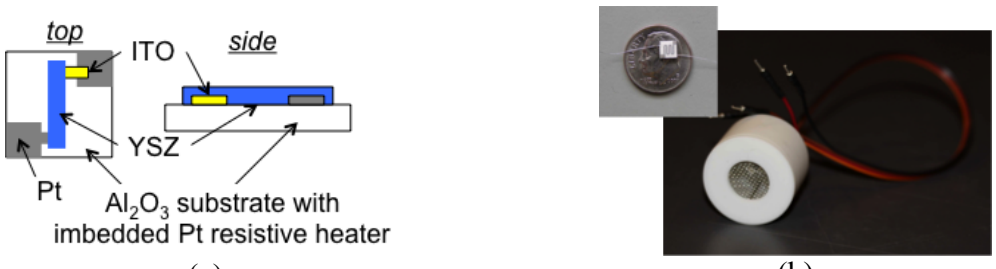

(a) (b)

Figure 3. (a) Schematic and (b) picture of electrochemical cell for the advanced prototype incorporating an on-chip embedded heater.

The specialized hydrogen sensor testing laboratory at NREL uses a variety of protocols to assess comparative sensor performance. The system can control and monitor temperature, pressure, humidity, and gas composition. In order to interface with the data collection system, the specialized high input impedance buffer board mentioned above was used. This board allowed correction of baseline offset and signal amplification.

Results and discussion

Mixed potential response

Figures 4a and 4b show results evaluating mixed potential sensor performance of the two different laboratory prototypes, YSZ-ITO/YSZ/LSM and Au/YSZ/Pt, respectively. The two sensors were tested side-by-side in the furnace, and Figs. 4a and 4b show the sensor signal for dynamic changes to different H_2 concentrations under dry conditions and in the presence of 10% water. While the nominal inlet water concentration was 10% and temperature was 70°C (relative humidity of ~33%), small variations occurred as measured by a humidity and temperature sensor (Sensirion) placed just before the furnace inlet.

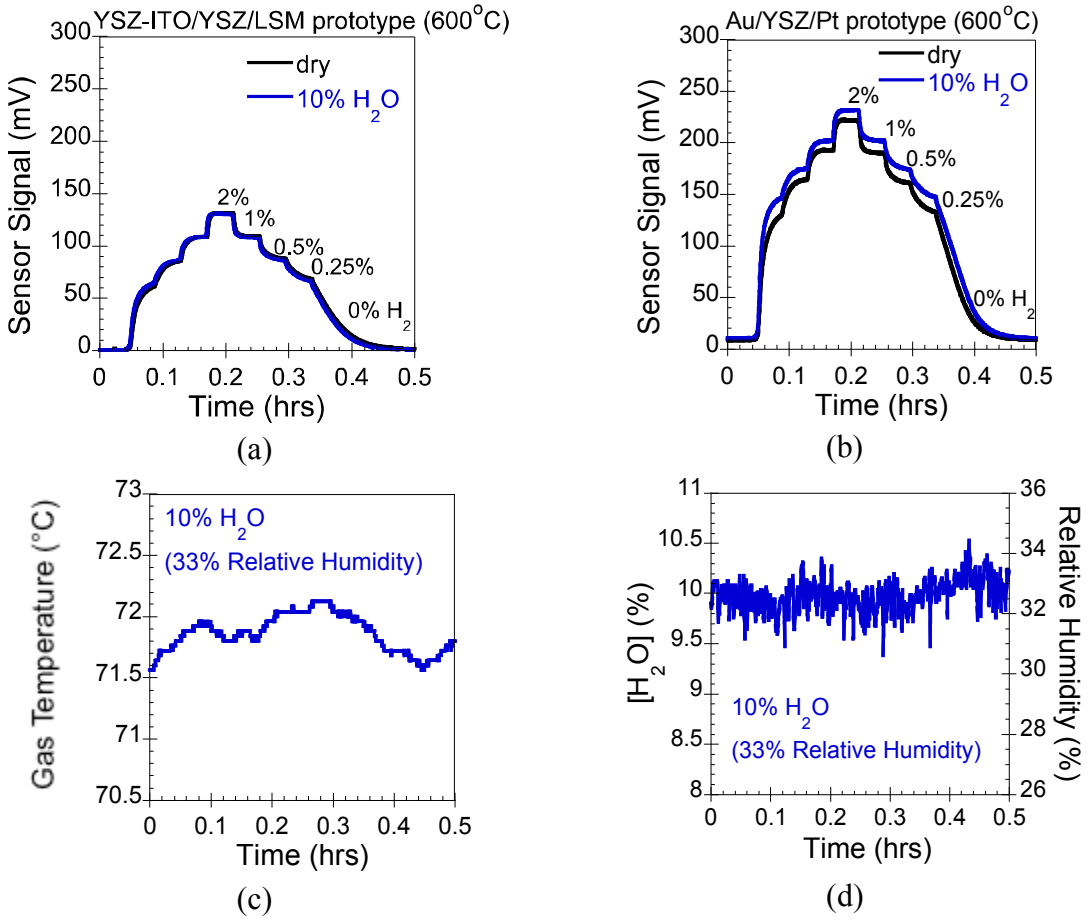

Figure 4. Mixed potential sensor response of (a) YSZ-ITO/YSZ/LSM and (b) Au/YSZ/Pt prototypes, with corresponding (c) gas temperature and (d) water concentration measurements during testing in the presence of 10% (nominal) water.

As shown in Fig. 4a, the YSZ-ITO/YSZ/LSM prototype had better tolerance to humidity, with the data under dry conditions and under wet conditions coinciding with each other. In contrast, the Au/YSZ/Pt prototype showed some humidity dependency (Fig. 4b). The overall signal magnitude of the hydrogen response was smaller for the YSZ-ITO/YSZ/LSM prototype compared to the Au/YSZ/Pt prototype, although the sensitivity

over the range of hydrogen concentrations was similar for the two prototypes, as shown by the fairly similar slopes (taken in different hydrogen concentration regions) of the sensor response vs. hydrogen concentration shown in Fig. 5.

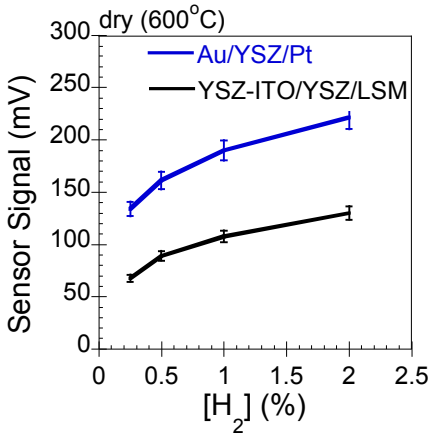

Figure 5. Hydrogen sensitivity of Au/YSZ/Pt and YSZ-ITO/YSZ/LSM prototype sensors under dry conditions.

Electrochemical Characterization

Figure 6 shows results for both impedance spectroscopy and voltammetry for the Au/YSZ/Pt prototype in air and in air with 2% H_2. Figure 6a shows impedance results in a complex plane plot with real impedance on the x-axis and negative imaginary impedance on the y-axis (Nyquist plot). The Nyquist plot shows two characteristic arcs in the frequency regime shown, which is from 100 kHz to 1 Hz. In Fig. 6a each datum represents a different frequency, and the darkened points and numbers correspond to log of frequency in Hz. Electrode polarization contribution to the overall impedance is represented by the lower frequency arc. As shown in Fig. 6a, there is a decrease in the diameter of this arc with the introduction of 2% H_2 to the gas stream.

A relationship exists between impedance and voltammetry measurements since impedance measurements use perturbations at small amplitude voltage excitations. Therefore, the DC resistance (R) in impedance measurements, as shown as the low-frequency arc intercept with the real axis (see Fig. 6a), corresponds to the inverse of the slope in the voltammetry plot around zero voltage. The discrete data points in the Nyquist plot are labeled R_{H2} and R_{air}, in correspondence to the inverse of the voltammetric slope, m_{H2} and m_{air} shown in Fig. 6b. The voltammetric slopes were obtained using a linear fit for the voltammetry data from -100 mV to 100 mV (shown by the dotted lines in Fig. 6b). It is noted from the voltammetric plots in Fig. 6b that the introduction of 2% H_2 resulted in a negative potential shift of the open circuit (zero current) potential. This is due to the reactions that occur on the two electrodes, with different apparent reaction rates.

Impedance Spectroscopy. Figure 7 shows the Nyquist plots for the two different laboratory prototypes in air and in air with 2% H_2 under dry conditions. For both sensors, the lower frequency electrode polarization arc diameter decreases with the introduction of 2% H_2. The YSZ-ITO/YSZ/LSM prototype had larger time constants for the electrode polarization, as indicated by the lower frequency at the top of the electrode polarization arc, as well as exhibiting increasing magnitude in the imaginary impedance for

frequencies approaching 1 Hz. The Nyquist behavior of the YSZ-ITO/YSZ/LSM prototype possibly indicates greater influence of diffusion and/or adsorption effects compared to the Au/YSZ/Pt prototype, which had higher frequencies at the top of the electrode polarization arc, indicating smaller time constants. The introduction of the beginning of a third arc for the ITO/YSZ/LSM sensor at the lowest frequencies probed could be indicative of diffusional processes.

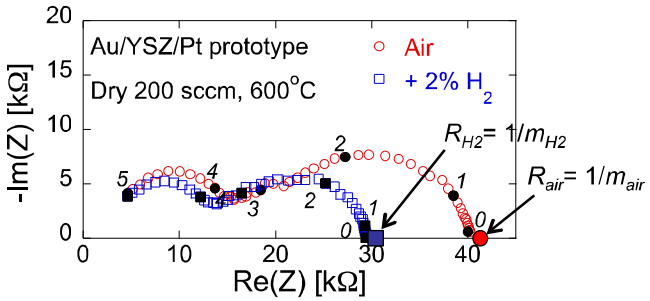

(a)

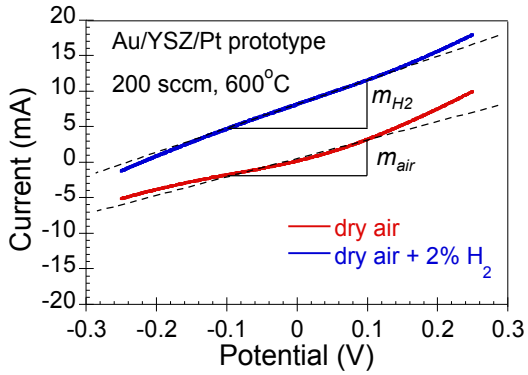

(b)

Figure 6. Measurements for the H_2 response of the Au/YSZ/Pt sensor using (a) impedance spectroscopy (where R is DC resistance and darkened points with corresponding numbers are log of frequency in Hz) and (b) cyclic voltammetry, where m is the slope of the voltammetry curve using a linear fit from -100 mV to 100 mV (shown as dotted lines).

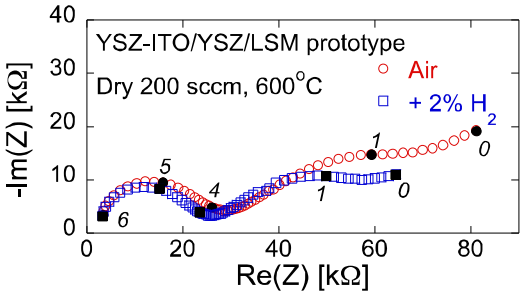

(a)

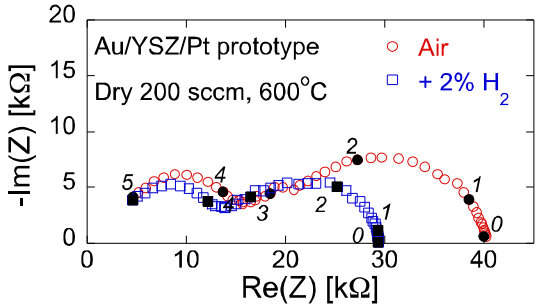

(b)

Figure 7. Nyquist plots in air and in air with 2% H_2 for (a) YSZ-ITO/YSZ/LSM and (b) Au/YSZ/Pt prototype.

Figure 8 shows the Nyquist plots for the two different prototypes in dry air and in air with 10% water. For the YSZ-ITO/YSZ/LSM prototype in Fig. 8a, which showed little mixed potential response to humidity changes (Fig. 4a), there was a decrease in the electrode polarization upon introduction of 10% water that was similar to the decrease noted with the introduction of 2% H_2 (Fig. 7a). For the Au/YSZ/Pt prototype (Fig. 8b), which did show measureable mixed potential response to water (Fig. 4b), the electrode polarization was relatively unaffected by changes in water concentration. While this may appear to be a contradiction, it can be explained by noting that impedance measurements are based on small enforced potential perturbations (± 100 mV) applied near the open circuit potential whereas the mixed potential is an open circuit measurement. The mixed potential is reflective of a differential balance in reaction rates for the relevant redox reactions on the two cell electrodes. The introduction of a new reactant (e.g., water) that can directly or indirectly influence reactions on the electrode surface can shift the equilibrium potential if there are differential effects on the two electrodes. In impedance measurements, the system is forced away from equilibrium, albeit within a small potential range. If there is no difference in measured impedance upon the introduction of a new gas component, this implies that there is no net electrode polarization changes for the system. Cyclic voltammetry provides additional information about reaction rates as is discussed below.

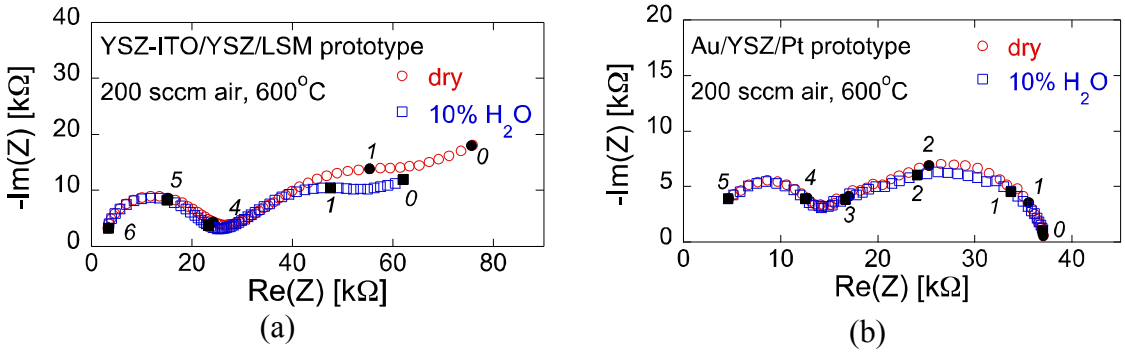

Figure 8. Nyquist plots in dry air and in air with 10% H_2O for (a) YSZ-ITO/YSZ/LSM and (b) Au/YSZ/Pt prototype.

Cyclic Voltammetry. Figure 9 shows cyclic voltammetry (CV) measurements for the Au/YSZ/Pt prototype. The CV curves showed no dependency on scan rates for 10, 50, and 100 mV/sec, and did not display hysteresis or peaks, which likely resulted from the small time constants of the electrode polarization noted previously in the impedance results. Also, there were minimal differences between the CV curves of the Au/YSZ/Pt prototype in dry air and in air with 10% water, which correlated with the minimal difference shown previously in the impedance measurements (Fig. 8b). The CV curves showed linear regimes in both the positive and negative potential regions at potentials greater than approximately 150 mV away from 0 V. The different slopes at positive and negative potentials indicate different rates for the reactions occurring in each region (see Eqs. 1 and 2), these reaction rates dominating mixed potential operation; which is a rather obvious result. Figure 9 also shows that with the addition of 2% H_2, the open circuit mixed potential (equilibrium) shifted to more negative potentials. Such an effect is reflected in the mixed potential measurement (Fig. 4b).

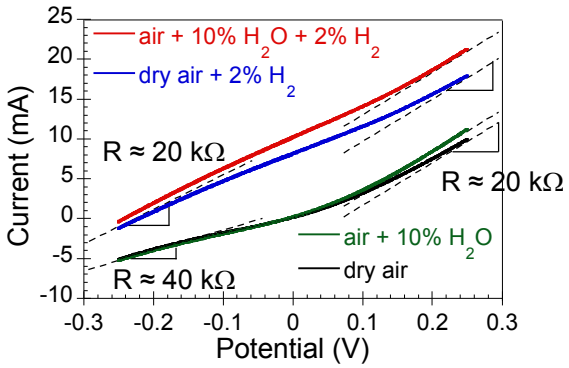

Figure 9. Cyclic voltammetry (CV) results shown in a current-potential plot for Au/YSZ/Pt prototype (200 sccm gas flow, 600 °C, and 100 mV/sec scan rate).

Figure 10 shows CV results for the YSZ-ITO/YSZ/LSM prototype. In contrast to the Au/YSZ/Pt prototype in Fig. 9, Fig. 10a shows a scan rate dependency as well as hysteretic behavior. These effects seem to indicate the influence of diffusion and/or adsorption effects that have larger time constants for ITO/YSZ/LSM (also noted earlier in the impedance results, Fig. 7a).

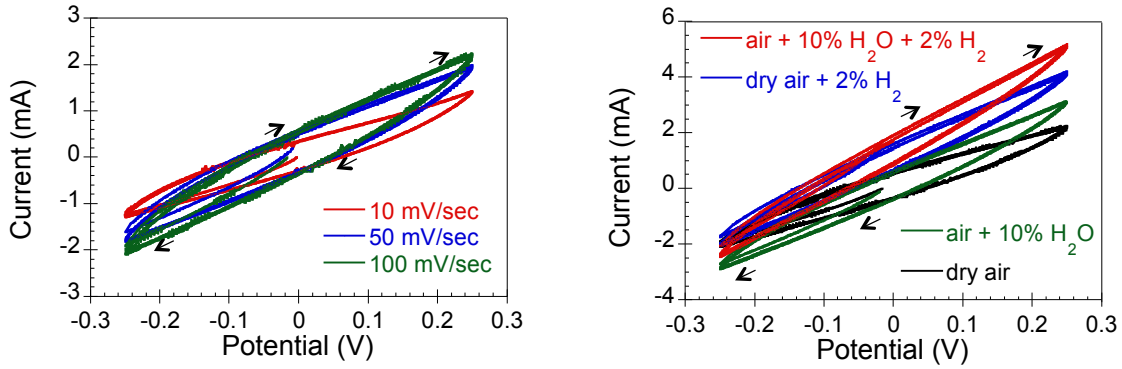

Figure 10. Cyclic voltammetry results shown for the YSZ-ITO/YSZ/LSM prototype (200 sccm gas flow and 600 °C) (a) for different scan rates in air under dry conditions and (b) for 100 mV/sec scan rate upon addition of hydrogen and water.

In Fig. 10, the YSZ-ITO/YSZ/LSM prototype showed CV behavior with more similar slopes, and therefore reaction rates, for the negative and positive potential regimes, under all conditions, with and without hydrogen, in dry and humid conditions. Therefore, the YSZ-ITO/YSZ/LSM behavior differed from the behavior noted for the Au/YSZ/Pt prototype, where quite different slopes were noted. Similar to the Au/YSZ/Pt prototype, with the addition of 2% H_2, the open circuit mixed potential response shifted to more negative potentials; although, for YSZ-ITO/YSZ/LSM the shift of open circuit potential is less pronounced than for Au/YSZ/Pt. This behavior is also reflected in the smaller mixed potential response of YSZ-ITO/YSZ/Pt to step changes in H_2 concentration (Fig. 4a).

Figure 11 shows the CV results for both prototypes in dry air and in air with 10% water. In Fig. 11a, the YSZ-ITO/YSZ/LSM prototype displayed more similar slopes in the positive and negative potential regimes with similar changes in both regimes with the

introduction of 10% water. The similar slopes in both regimes, indicating similar reaction rates, may indicate that any influence of humidity would be minimized since the mixed potential difference between the two electrodes would remain relatively unchanged. Therefore, the mixed potential performance of the YSZ-ITO/YSZ/LSM prototype had good tolerance to humidity with almost identical hydrogen response under dry conditions and with the introduction of 10% water (Fig. 4a).

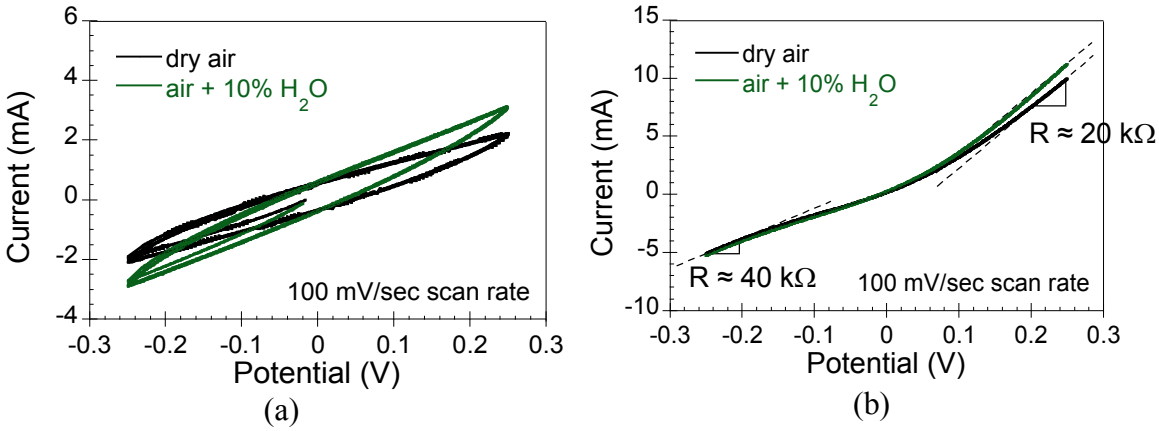

Figure 11. Cyclic voltammetry results shown in dry air and in air with 10% water (200 sccm gas flow and 600 °C) for (a) YSZ-ITO/YSZ/LSM and (b) Au/YSZ/Pt prototype.

In Fig. 11b, the Au/YSZ/Pt prototype displayed two different linear regions in the positive and negative potential regimes under dry conditions and with the introduction of 10% water. Additionally, there is a small change in the CV curve in the positive potential regime in dry air with the introduction of 10% water. With the introduction of hydrogen, under dry or wet conditions, the linear regions in the positive and negative potential regimes displayed more similar slopes, as shown in Fig. 9, indicating that the presence of hydrogen had a larger influence on reaction rates in the negative potential regime compared to the positive potential regime. In contrast, in the YSZ-ITO/YSZ/LSM prototype, additions of either water or hydrogen resulted in more similar slope changes in both the positive and negative potential regimes. The larger influence of hydrogen on reaction rates in the negative potential regimes in combination with the small change in the positive potential regime in dry air with the introduction of 10% water could explain the presence of a larger mixed potential signal (difference in reaction rates between the two electrodes) when both hydrogen and water are present and the resulting poor humidity tolerance in the Au/YSZ/Pt prototype. Additional studies are necessary to further elucidate the mechanisms responsible for the effect of humidity.

Miniaturized Packaged Prototypes

As described in the experimental section, more advanced ITO/YSZ/Pt prototypes were also developed in parallel work for testing on the specialized hydrogen sensor test stand developed at NREL. The advanced prototypes were developed to demonstrate miniaturization using thin film deposition techniques and robustness for cross-validation testing. This will advance the technology towards testing in more realistic environments and in the field.

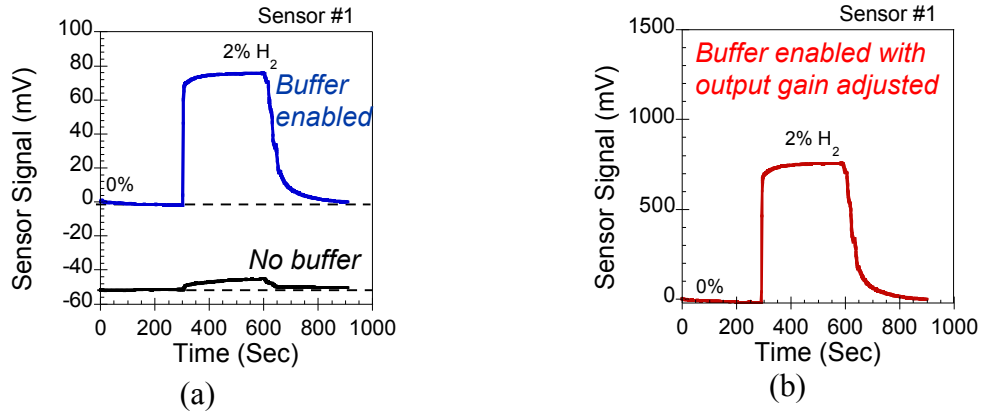

Figure 12. Mixed potential sensor performance of more advanced ITO/YSZ/Pt prototype showing (a) effect of buffer electronics to remove anomalous baseline and recover sensitivity and (b) effect of buffer electronics to magnify the output gain.

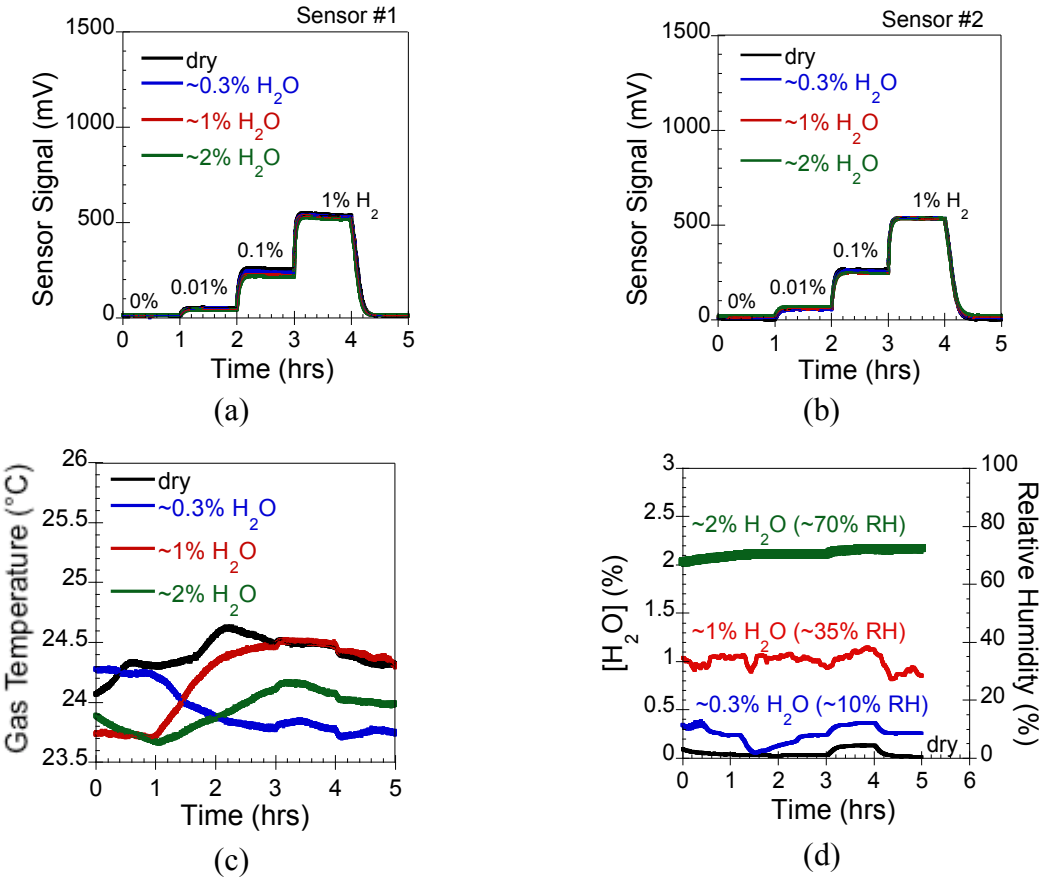

Figure 13. Mixed potential sensor performance of more advanced ITO/YSZ/Pt prototypes, (a) Sensor #1 and (b) Sensor #2, with corresponding (c) gas temperature and (d) water concentration measurements under dry conditions and in the presence of ~0.3, ~1, and ~2% water.

For the evaluation of the more advanced miniaturized packaged prototype, the specialized data acquisition system required the development of additional electronics for compatibility with the NREL measurement equipment. A raw sensor response using the available data acquisition system at NREL indicated an anomalous baseline (-50 mV) with small response magnitude (bottom curve, Fig. 12a). The appearance of the artifacts measured by the data acquisition system was confirmed using a stand-alone digital multimeter. High impedance buffer board electronics were necessary to protect the sensor response, remove the artificial offsets, and clarify sensor response (top curve in Fig. 12a). The buffer also provided an additional capability of adjusting the output gain to increase signal-to-noise, which is shown in Fig. 12b, with mixed potential response magnitudes as high as 750 mV in air with 2% H_2.

Figure 13 shows the mixed potential sensor performance of more advanced prototypes, with two sensors (Sensor #1 and Sensor #2) tested side-by-side in the NREL test stand using separate buffer electronics with the output gain adjusted. In Figs. 13a and 13b, the mixed potential sensors show good and reproducible response to hydrogen in the concentration range of 0.01-1% in both dry conditions and in the presence of water up to 2%. To monitor system environmental variability from nominal set parameters, a humidity sensor and thermocouple continuously monitored water and temperature in the chamber (Figs. 13c and 13d).

Conclusion

Electrochemical characterization studies were performed using two different solid-state electrochemical hydrogen safety sensor prototypes, an electrochemical cell that consisted of only oxide materials (YSZ-ITO/YSZ/LSM), and a cell with metal electrodes (Au/YSZ/Pt). Both prototypes showed mixed potential response to dynamic changes in hydrogen from 0.25 to 2% H_2; however, YSZ-ITO/YSZ/LSM showed minimal cross-sensitivity to 10% water while Au/YSZ/Pt demonstrated poor humidity tolerance. Impedance spectroscopy and cyclic voltammetry indicated that similar reaction rates for negative and positive potential regimes for the YSZ-ITO/YSZ/LSM prototype could be responsible for humidity tolerance.

Sensor prototypes were also developed to demonstrate miniaturization and robust packaging for cross-validation testing in an advanced test environment. These sensors used both metal oxide and metal electrodes, and had an ITO/YSZ/Pt cell structure. For compatibility with available measurement and data acquisition systems, which is not standard laboratory electrochemical equipment, a high impedance buffer board was developed to interface directly to the sensors. These prototypes were tested side-by-side with commercially available sensors in a specialized hydrogen sensor test environment. These prototypes demonstrated good performance over a range of hydrogen concentrations from 0.01-1% in both dry conditions and in the presence of water up to 2%.

Acknowledgments

The authors wish to acknowledge support from the Department of Energy, Fuel Cells Technologies Program, and the Program Manager Antonio Ruiz. This work was performed under the auspices of the U.S. Department of Energy by Lawrence Livermore National Laboratory under Contract DE-AC52-07NA27344.

References

1. W.J. Buttner, M.B. Post, R. Burgess, C. Rivkin, *Int. J. Hydrogen Energy*, **36**, 2462 (2011).
2. L. Boon-Brett, J. Bousek, G. Black, P. Moretto, P. Castello, T. Hu□bert, and U. Banach, *Int. J. Hydrogen Energy*, **35**, 373 (2010).
3. L.P. Martin, A-Q. Pham, R.S. Glass, *Solid State Ionics*, **175**, 527 (2004).
4. L.P. Martin and R.S. Glass, *J. Electrochem. Soc.*, **152**, H43 (2005).
5. P.K.Sekhar, E.L.Brosha, R. Mukundan, T. L. Williamson, M.A.Nelson and F.H.Garzon, *Sensor Actuat. B-Chem.*, **148**, 469 (2010).
6. E.L.Brosha, P.K.Sekhar, R.Mukundan, T.L.Williamson, F.H.Garzon, L.Y.Woo, and R.S.Glass, *ECS Trans.*, **26** (1), 475 (2010).
7. J.W. Fergus, *J. Solid State Electrochem.*, **15**, 971 (2011).